

# PCCP

Accepted Manuscript

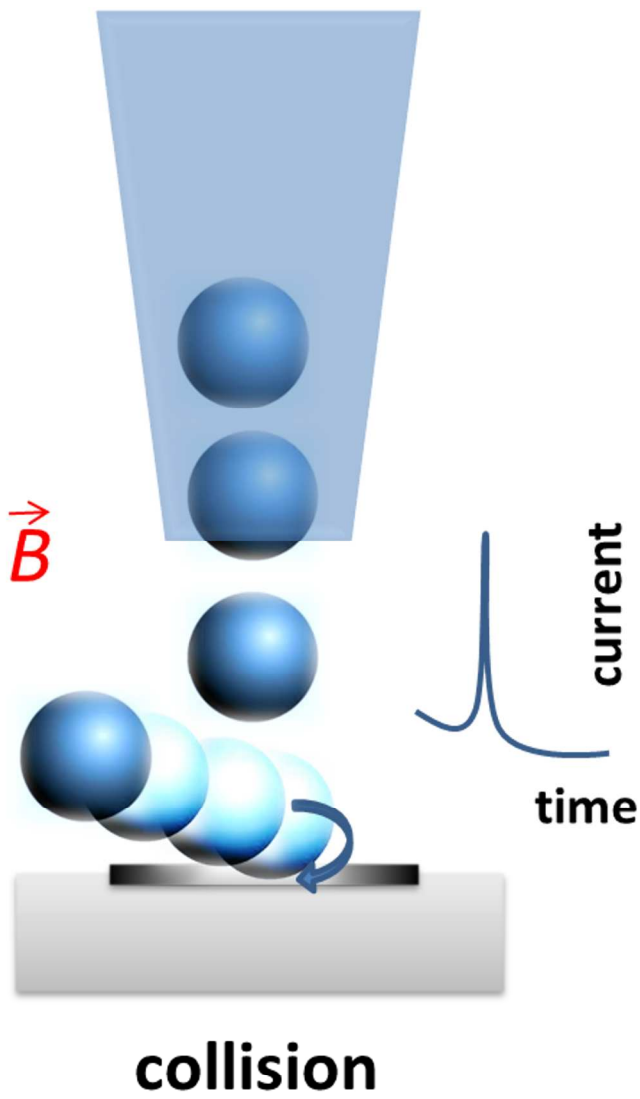


This is an *Accepted Manuscript*, which has been through the Royal Society of Chemistry peer review process and has been accepted for publication.

*Accepted Manuscripts* are published online shortly after acceptance, before technical editing, formatting and proof reading. Using this free service, authors can make their results available to the community, in citable form, before we publish the edited article. We will replace this *Accepted Manuscript* with the edited and formatted *Advance Article* as soon as it is available.

You can find more information about *Accepted Manuscripts* in the [Information for Authors](#).

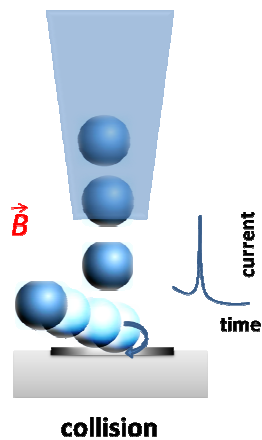
Please note that technical editing may introduce minor changes to the text and/or graphics, which may alter content. The journal's standard [Terms & Conditions](#) and the [Ethical guidelines](#) still apply. In no event shall the Royal Society of Chemistry be held responsible for any errors or omissions in this *Accepted Manuscript* or any consequences arising from the use of any information it contains.



635x1063mm (96 x 96 DPI)

## Graphical Abstract

By applying a magnetic field close to a gold microelectrode, collisions of magnetite nanoparticles modified with Prussian could be controlled.



# Magnetically controlled single-nanoparticle detection via particle–electrode collisions

Germano P. Santos, Antonio F. A. A. Melo, Frank N. Crespilho\*

Received (in XXX, XXX) Xth XXXXXXXXXX 200X, Accepted Xth XXXXXXXXXX 200X

5 First published on the web Xth XXXXXXXXXX 200X

DOI: 10.1039/b000000x

This paper reports the magnetic control of nanoparticle collisions on gold ultramicroelectrode surfaces. Magnetite nanoparticles with diameters of 10 nm and modified with Prussian blue (NPs-Fe<sub>3</sub>O<sub>4</sub>-PB) were directed by gravitational force on the electrode surface, and spikes in  
10 current–time transients were observed. By modulating a magnetic field parallel to the electrode surface, the number of nanoparticle collisions and the nanoparticle positions could be controlled.

## 1. Introduction

15 Collisions of NPs on electrode surfaces have attracted much interest in recent years.<sup>1–5</sup> The pioneering work came from Bard's group; they showed the collisions of individual platinum NPs at an UME in current–time transients for a particle-catalyzed reaction.<sup>1</sup> They correctly proposed that every collision produces a  
20 unique current–time profile related to the particle size, particle residence time, and the nature of particle interaction with the electrode surface, thus opening many possibilities in surface science. More recently, Compton and co-workers<sup>2</sup> successfully demonstrated the use of particle coulometry to monitor the  
25 collisions of tagged AuNPs; they proposed that it has considerably wide application in analytical nanoscience, microfluidics, nanodrug formulation and delivery. Crooks and co-workers<sup>3</sup> showed the optical tracking of collisions between insulating microbeads and an UME surface in experiments that  
30 were based on partial blocking of the electrode surface by the beads. In addition to the above examples, various groups have reported many important results in the last few years,<sup>4–10</sup> usually involving collisions of insulating particles<sup>3</sup> or the generation of signals through electrocatalytic amplification.<sup>5</sup>

35 In this paper, we introduce a new approach that uses an external magnetic field to control the particle–electrode collisions. We believe that the most important discovery is that electrochemical signals can be modulated by applying an external magnetic field to an electrode surface. To the best of our  
40 knowledge, magnetically controlled electrochemical single events have not been studied before.

## 2. Materials and methods

### 2.1 Chemicals

55 Ferric chloride hexahydrate 99% (FeCl<sub>3</sub>·6H<sub>2</sub>O), ferrous chloride tetrahydrate 99% (FeCl<sub>2</sub>·4H<sub>2</sub>O), potassium ferricyanide 99% (K<sub>3</sub>[Fe(CN)<sub>6</sub>]), sodium hydroxide 98% (NaOH) and hydrochloric acid 37% (HCl) were purchased from Sigma-Aldrich. Potassium  
60 phosphate dihydrate (KH<sub>2</sub>PO<sub>4</sub>) and potassium phosphate monohydrate (K<sub>2</sub>HPO<sub>4</sub>) used in the preparation of 0.1 mol L<sup>-1</sup> supporting electrolyte (pH 7.2) were purchased from Vetec. All solutions were prepared from chemical of high purity and ultra-pure water (Milli-Q, 18.2 MΩ cm<sup>-1</sup>).

### 2.2 Preparation of ultramicroelectrode (Au UME)

65 Gold ultramicroelectrode (10 μm diameter) was firstly rinsed with water and ethanol, and then, polished with alumina powder  
70 water suspension (0.05 microns). At last, the ultramicroelectrode was subjected to 100 voltammetric cycles in 0.1 mol L<sup>-1</sup> H<sub>2</sub>SO<sub>4</sub> solution between 0 and 1.0 V vs. Ag/AgCl.

### 2.3 Synthesis and characterization of NPs-Fe<sub>3</sub>O<sub>4</sub> modified with Prussian blue (PB)

75 NPs-Fe<sub>3</sub>O<sub>4</sub> were synthesized by the coprecipitation method as reported in the literature.<sup>11</sup> For this, FeCl<sub>3</sub>·6H<sub>2</sub>O (5.4 g) and FeCl<sub>2</sub>·4H<sub>2</sub>O (2.0 g) were subsequently dissolved in 25 mL of a  
80 10 mmol L<sup>-1</sup> HCl solution, and then 250 mL of 1.5 mol L<sup>-1</sup> NaOH solution were added dropwise to this mixture with vigorous stirring (20 rpm) at 80 °C under N<sub>2</sub> atmosphere. NPs-Fe<sub>3</sub>O<sub>4</sub> in suspension were separated by magnetism and then washed with distilled water several times until pH 6.4. At last, NPs-Fe<sub>3</sub>O<sub>4</sub>  
85 were dispersed in 500 mL of 0.01 mol L<sup>-1</sup> HCl (stock suspension of NPs-Fe<sub>3</sub>O<sub>4</sub>).

45  
Instituto de Química de São Carlos, Universidade de São Paulo, CEP: 780, 13560-970 São Carlos-SP, Brazil; Tel.: +55 16 3373 6653; E-mail: frankcrespilho@iqsc.usp.br

For modification with PB, firstly NPs-Fe<sub>3</sub>O<sub>4</sub> present in 10 mL of stock suspension were magnetically decanted, separated from the supernatant and then dispersed in 5 mL of 0.1 mol L<sup>-1</sup> FeCl<sub>2</sub>·4H<sub>2</sub>O solution. After, 5 mL of 0.1 mol L<sup>-1</sup> K<sub>3</sub>[Fe(CN)<sub>6</sub>] solution were added dropwise, which leads to the formation of a dark blue precipitate. Finally, NPs-Fe<sub>3</sub>O<sub>4</sub> coated with PB (NPs-Fe<sub>3</sub>O<sub>4</sub>-PB) were magnetically decanted, washed to remove non-adsorbed PB (this procedure was repeated three times) and dispersed in 250 mL of distilled water - stock suspension of NPs-Fe<sub>3</sub>O<sub>4</sub>-PB (0.42 mg mL<sup>-1</sup>).

## 2.4 Instrumentation

TEM images of NPs-Fe<sub>3</sub>O<sub>4</sub> were obtained with a FEI Tecnai G2 F20 equipped operated at 200 kV. The interaction between PB and NPs-Fe<sub>3</sub>O<sub>4</sub> surface was investigated by FTIR using a Shimadzu IRAffinity-1 Spectrometer with window of potassium bromide (KBr). For study of collisions of NPs-Fe<sub>3</sub>O<sub>4</sub>-PB were used chronoamperometry experiments in the presence of a magnet. For this, an Autolab PGSTAT 128N potentiostat/galvanostat coupled to the ECD module for low current measurements was employed. Platinum wire was used as counter electrode and Au UME was employed as work electrode. Figure 1 show experimental apparatus (cell and electrodes) used in the study of collisions of NPs-Fe<sub>3</sub>O<sub>4</sub>-PB.

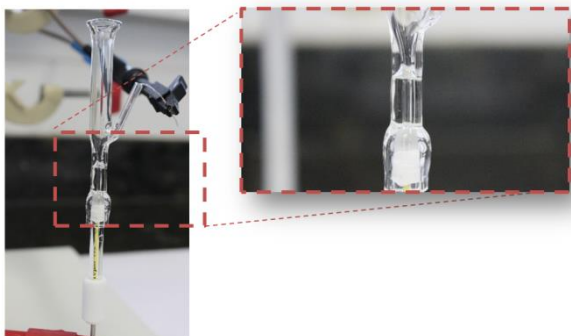


**Fig. 1** Images of experimental apparatus used in the study of collisions of NPs-Fe<sub>3</sub>O<sub>4</sub>-PB.

## 3. Results and discussion

### 3.1 Characterization of Nps-Fe<sub>3</sub>O<sub>4</sub> and PB modified-nanoparticles

NPs-Fe<sub>3</sub>O<sub>4</sub> were obtained by co-precipitation method and then modified with Prussian blue (PB) based in the method proposed by Melo and co-workers.<sup>12</sup> The average diameter of NPs-Fe<sub>3</sub>O<sub>4</sub> observed in the TEM image (Fig. 2a) was 10.9 nm with a degree of polydispersity ( $\sigma$ ) of 2.3%. This indicates that NPs-Fe<sub>3</sub>O<sub>4</sub> are monodisperse in spite of have not completely spherical morphology.

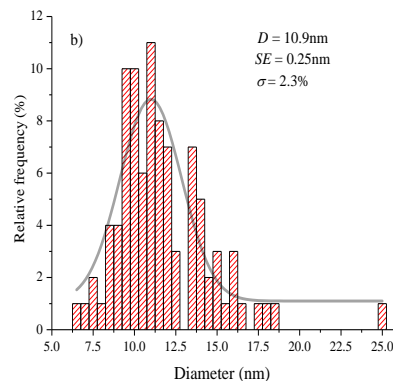
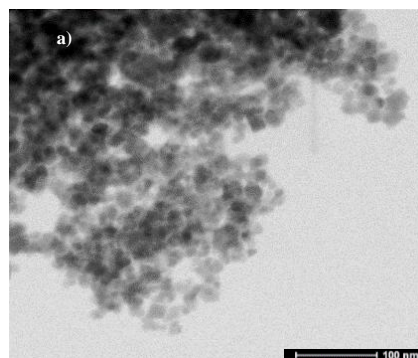


**Fig. 2** a) TEM Images of NPs-Fe<sub>3</sub>O<sub>4</sub>. b) Histogram and gaussian fit to diameter distribution of NPs-Fe<sub>3</sub>O<sub>4</sub>.

As previously reported, NPs-Fe<sub>3</sub>O<sub>4</sub> were modified with Prussian blue. FTIR was used to confirm this modification and the PB distribution in several nanoparticles was observed by using *in situ* EDX. Figure 3 shows images of NPs-Fe<sub>3</sub>O<sub>4</sub>-PB in aqueous suspension (left side) and NPs-Fe<sub>3</sub>O<sub>4</sub>-PB grouped after the application of external magnetic field (rightside).

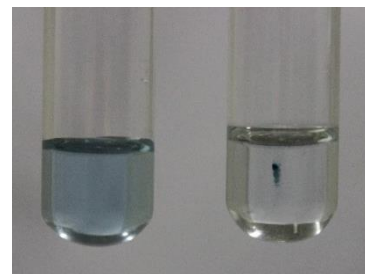


**Fig. 3** Images of NPs-Fe<sub>3</sub>O<sub>4</sub>-PB in aqueous suspension (left side) and NPs-Fe<sub>3</sub>O<sub>4</sub>-PB grouped after the application of external magnetic field (right side).

Figure 4 shows FTIR spectra of NPs-Fe<sub>3</sub>O<sub>4</sub> (black line) and NPs-Fe<sub>3</sub>O<sub>4</sub>-PB (blue line). For the NPs-Fe<sub>3</sub>O<sub>4</sub> spectra was observed the presence of two peaks at 445 and 632 cm<sup>-1</sup> corresponding to vibrations of the Fe-O and Fe-O-Fe bonds, respectively. The peak of medium intensity at 2075 cm<sup>-1</sup> was assigned to the CN stretching of formed structure [Fe<sup>2+</sup>-CN-Fe<sup>3+</sup>], NPs-Fe<sub>3</sub>O<sub>4</sub>-PB spectra. Also, the absorption bands at 3415 and 1627 cm<sup>-1</sup> are attributed to -OH stretching and H-O-H

deformation, respectively, indicating the presence of water molecule.<sup>12</sup>

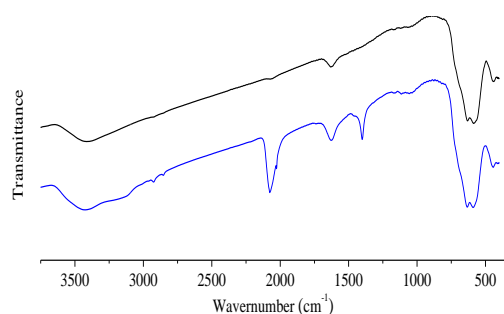


**Fig. 4** FTIR spectra of NPs-Fe<sub>3</sub>O<sub>4</sub> (black line) and NPs-Fe<sub>3</sub>O<sub>4</sub>-PB (blue line).

In order to verify if all the NPs-Fe<sub>3</sub>O<sub>4</sub> are coated, or just a fraction, we have isolated several PB modified-nanoparticles by TEM, and *in situ* EDX measurements were carried out for several of them (about 10 different regions on Cu grid). For that, we observed the same signal intensity corresponding to PB, which suggests homogeneous distribution of PB molecules onto NPs-Fe<sub>3</sub>O<sub>4</sub> (see Supporting Information). This latter is statistic evidence that the most of the particles are modified. The amount of molecules of PB onto NPs-Fe<sub>3</sub>O<sub>4</sub> was obtained by chronoamperometry and compared by cyclic voltammetry (area integration), as shown in Figure 5.

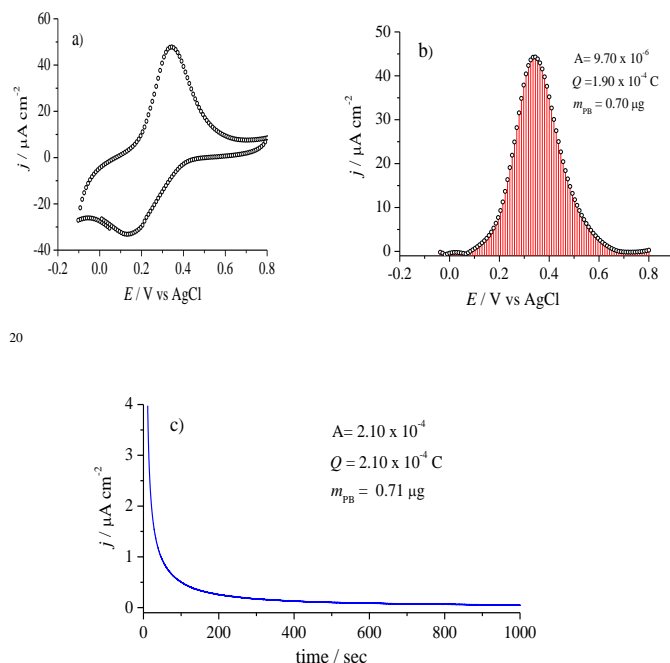


**Fig. 5** a) Cyclic voltammogram of NPs-Fe<sub>3</sub>O<sub>4</sub>-PB/ITO film (filme obtained by deposition of 50  $\mu\text{L}$  of the suspension of NPs-Fe<sub>3</sub>O<sub>4</sub>-PB). Scan rate: 50  $\text{mV s}^{-1}$ . b) Integration of the oxidation curve of cyclic voltammogram of NPs-Fe<sub>3</sub>O<sub>4</sub>-PB/ITO film. c) Current *versus* time transient NPs-Fe<sub>3</sub>O<sub>4</sub>-PB/ITO film. Applied potential:  $E_{\text{Oxd}} = 0.12 \text{ V}$ . Electrolyte: 0.1  $\text{mol L}^{-1}$  potassium phosphate buffer, pH 7.2.

For both experiments, the results were practically the same. For each 50  $\mu\text{L}$  of NPs-Fe<sub>3</sub>O<sub>4</sub>-PB (21  $\mu\text{g}$ ) dropped on 1  $\text{cm}^2$  ITO electrode, the oxidation curve yielded a value of  $2 \times 10^{-4} \text{ C}$ , which corresponds to 0.7842  $\mu\text{g}$  of PB. Therefore, the percentage (weight) of PB on NP-Fe<sub>3</sub>O<sub>4</sub>-PB was 3.7%. This suggests that only a few layers of adsorbed-PB are coated on magnetite nanoparticles surfaces. Furthermore, by x-ray diffraction it was verified the absence of PB crystals (data not shown). Thus, there is no considerable change in average diameter of NPs-Fe<sub>3</sub>O<sub>4</sub> after modification with PB, as can be seen in the TEM images (Fig. S1).

### 3.2 Scattering experiments and sedimentation time for NPs-Fe<sub>3</sub>O<sub>4</sub>-PB

The sedimentation velocity of NPs-Fe<sub>3</sub>O<sub>4</sub>-PB was determined by light scattering employing a fixed wavelength at 620 nm, as shown in Figure 6b. For this, 50  $\mu\text{L}$  of stock suspension of NPs-Fe<sub>3</sub>O<sub>4</sub>-PB (0.42  $\text{mg mL}^{-1}$ ) were added on top of the capillary and as expected the decantation of NPs-Fe<sub>3</sub>O<sub>4</sub>-PB occurred rapidly and unevenly (heavier particles settle out first). The average velocity of sedimentation was 6  $\text{mm min}^{-1}$  (Fig. 7b). Figure 6a shows representation of the kinetics of NPs-Fe<sub>3</sub>O<sub>4</sub>-PB sedimentation.

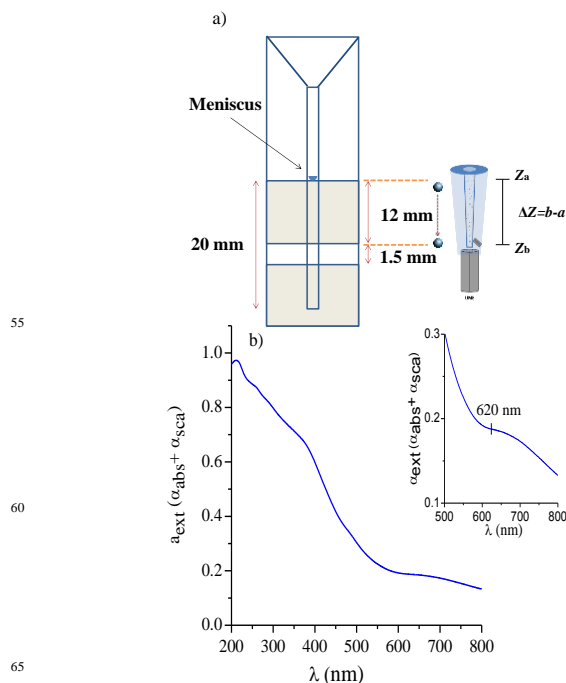


**Fig. 6** a) Schematic representation of the kinetics of NPs-Fe<sub>3</sub>O<sub>4</sub>-PB sedimentation (capillary height: 12 mm, cell volume: 350  $\mu\text{L}$  of 0.1  $\text{mol L}^{-1}$  potassium phosphate buffer + 50  $\mu\text{L}$  of 0.42  $\text{mg mL}^{-1}$  NPs-Fe<sub>3</sub>O<sub>4</sub>-PB suspension). b) UV-Vis spectrum of the NPs-Fe<sub>3</sub>O<sub>4</sub>-PB. *Inset*: intervalence band related to the absorption of Prussian blue in 620 nm.

Although the scattering sedimentation time is fast, some small NPs remain in suspension for a considerable time, around



100 minutes as shows in Figure 7a. Two regions are observed in the scattering spectrum. In (i), there is the initial process of sedimentation of NPs-Fe<sub>3</sub>O<sub>4</sub>-PB. In (ii), there is a steady-state where the particles are suspended in a long-term stability range.

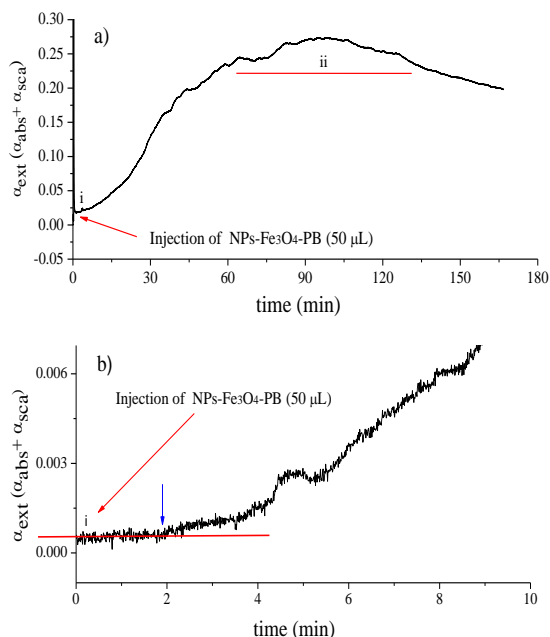


**Fig. 7** a) Long-term stability of NPs-Fe<sub>3</sub>O<sub>4</sub>-PB. b) Sedimentation time for NPs-Fe<sub>3</sub>O<sub>4</sub>-PB in fixed-wavelength of 620 nm (blue arrow).

### 3.3 Detection of particle–electrode collisions

For study of collisions of NPs-Fe<sub>3</sub>O<sub>4</sub>-PB it was employed a microcell with two electrodes: a gold UME (diameter = 10 μm) was used as the working electrode and a Pt wire was used as the counter electrode. Inside of the microcell, a capillary (0.5 mm in diameter and 2.0 cm in length) was positioned at a distance of 0.5 mm away from the basal plane of the UME. The cell and capillary were filled with the electrolyte. On top of the capillary, 50 μL aliquots of the NPs-Fe<sub>3</sub>O<sub>4</sub>-PB suspension (0.42 mg mL<sup>-1</sup>) were added and the current–time transient signal was recorded at different time intervals. A magnet was positioned parallel to the plane of the electrode. It had a maximum magnet field capacity of 0.2 T, as determined by a Gauss-meter (MagMeter MGM-20). It was possible to vary the magnetic field on the electrode surface by moving the magnet along the electrode. The field values used were 0.0, 0.1, and 0.2 T. When no magnetic field was applied (0.0 T), the particles descended on the electrode owing to the force of gravity, and collisions were recorded (Fig. 8c). In this case, the Mason–Weaver model<sup>13</sup> describes the sedimentation and diffusion of small particles, with a concentration (*c*) under a uniform gravitational acceleration (*g*) aligned in the *z* direction with the convective flux (*J*) owing to the terminal velocity (*v*<sub>term</sub>) of the particles. Based on the mathematical theory, Mason and Weaver believed that small particles immersed in a liquid

experience a motion that is the combination of a steady gravitational drift and Brownian movement.<sup>13</sup> In the case of the system reported here, we can conclude that the force of gravity was larger than other forces since fast particle sedimentation was observed. Figure 8a shows a scheme of the typical forces acting on a nanoparticle of mass *m* moving with vertical velocity *v*. These forces include the drag force (*fV*), the force of gravity (*mg*), and the buoyant force (*ρVg*), where *V* is the nanoparticle volume and *r* is the solvent density. At equilibrium, the nanoparticle attains a terminal velocity *v*<sub>term</sub> and the three forces are balanced. However, the density of magnetite is 5.2 g cm<sup>-3</sup>,<sup>14</sup> which caused the NPs to sink to the bottom of the electrochemical cell. Thus, when 50 μL were added on top of the capillary, the average velocity of decantation was 6 mm min<sup>-1</sup>. When there is a magnetic force (*F<sub>B</sub>*) parallel to the electrode plane, the ferromagnetic nanoparticle can be moved away from electrode surface according to the direction of the magnetic field (*B*), Figure 8c.

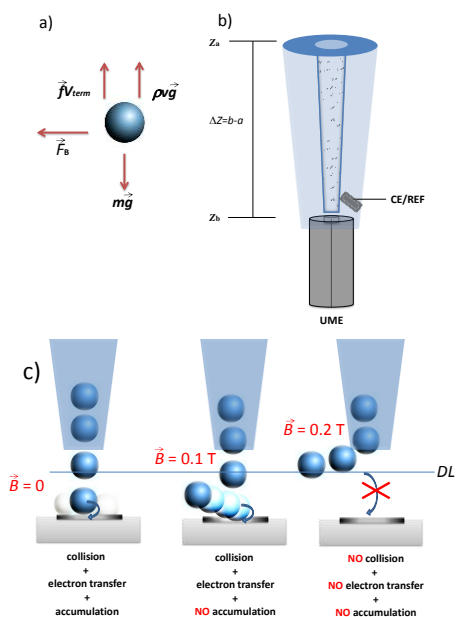


**Fig. 8** a) Typical forces acting on a nanoparticle of mass *m* moving with vertical velocity *v*: drag force *fV*; force of gravity *mg*; buoyant force *ρVg*. The nanoparticle attains a terminal velocity *v*<sub>term</sub> at equilibrium, and the three forces are balanced. A magnetic force *F<sub>B</sub>* parallel to the electrode plane can move the ferromagnetic nanoparticle away from the electrode surface according to the direction of the magnetic field *B*. b) Schematic representation of a capillary coupled with an UME. The injection of NPs-Fe<sub>3</sub>O<sub>4</sub>-PB with diameters of 10 nm occurs on top of the capillary, and the NPs traverse a distance of *Z<sub>b</sub>* - *Z<sub>a</sub>* and collide with the electrode surface. c) There are three scenarios, as shown from left to right: (Left) when no magnetic field is applied, and NPs collide and accumulate on electrode. (Center) When a magnetic field of 0.1 T is applied, there are collisions but no accumulation occurs. (Right) With a high magnetic field (0.2 T), no collision or accumulation occurs.

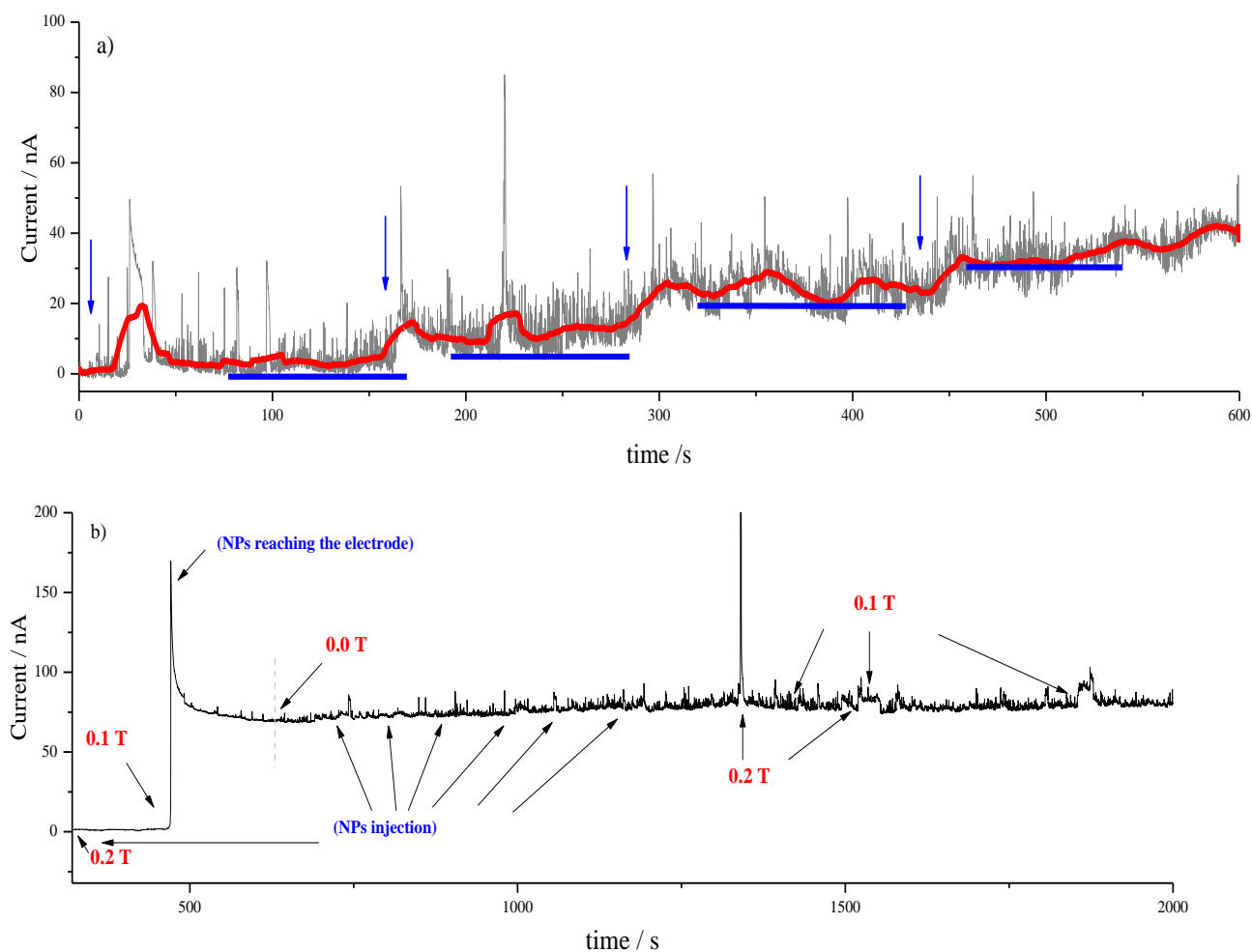


**Fig. 9** a) Current–time transients for particle collisions (applied potential: 0.12 V) with different injections of NPs and in the absence of an external magnetic field. b) Long-term (2000 s) current–time transients for particle collisions under different conditions. The arrows with red text indicate the positions when a magnetic field was applied.

Figure 9a shows the current–time transients for the NPs- $\text{Fe}_3\text{O}_4$ -PB in the absence of an external magnetic field. Collisions of the NPs were observed on the electrode surface. The redox processes are attributed to the one-electron transfer between Prussian blue and Prussian white (PW) owing to the overpotential applied of 0.12 V.<sup>15</sup> When a magnetic field was absent, the NPs- $\text{Fe}_3\text{O}_4$ -PB collided against the electrode surface. The observed increase in faradaic current was associated with each injection of the NPs-containing aliquot (blue arrows), which confirmed that the NPs were reacting in the electrode. However, they were not removed from the electrode, and as time passed, more NPs- $\text{Fe}_3\text{O}_4$ -PB arrived and accumulated on the electrode. For the first 300 s of the experiment, the time duration for a spike current (from the beginning of a collision to the end of current registration) was 0.3 s, so we can infer that the duration ( $\Delta t$ ) for each collision was 0.3 s. The frequency of collisions was related to one spike current every 13 s; however, the number of spikes decreased.

The decrease was more drastic after 300 s, suggesting that the electrode was less sensitive to collisions, probably because of the accumulation of NPs- $\text{Fe}_3\text{O}_4$ -PB on its surface. Although the number of spikes decreased, the total current continued to increase, and it can be attributed to the amount of NPs that had already aggregated on the surface. The red line in Figure 9a shows that there were increases in the current–time transients. This line was obtained by eliminating the spikes to yield smoothed current signals, where the smoothed value at index  $i$  was the average of data points in the interval  $[i-(n-1)/2, i+(n-1)/2]$ . The quasi-steady state current, represented by the blue line, appeared after the NPs- $\text{Fe}_3\text{O}_4$ -PB aliquot injections, similar to a traditional chronoamperogram; the total current increased from 0 to 600 s. Based on the findings from Crooks and co-workers,<sup>3</sup> the phenomena of local collision and NPs- $\text{Fe}_3\text{O}_4$ -PB aggregation on an active UME were related to the magnitude of the resulting current steps; the collisions and aggregation were also observed in optical tracking and simulations of experiments.

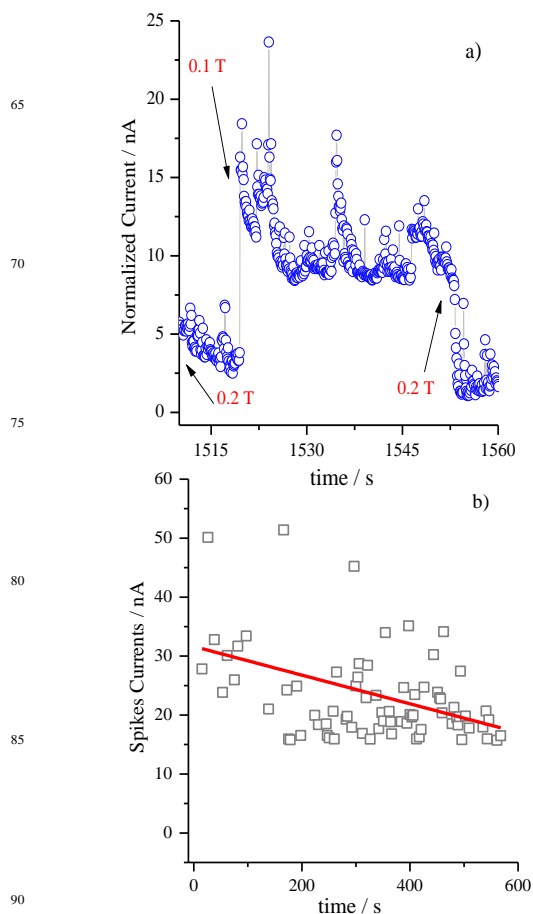


Figure 9b shows a typical current–time transient obtained when a magnetic field of 0.1 or 0.2 T was applied parallel to the plane of the electrode. In this case, we have three different scenarios. When the field was applied with low intensity (0.1 T) the NPs-Fe<sub>3</sub>O<sub>4</sub>-PB did not accumulate on the surface of the UME. Consequently, there were just current spikes resulting from collisions and the total current did not increase over a period of 630 s. Although the NPs-Fe<sub>3</sub>O<sub>4</sub>-PB collided with the surface, they were removed owing to the presence of a magnetic field. On the other hand, when the magnetic field was removed, the NPs-Fe<sub>3</sub>O<sub>4</sub>-PB began to accumulate on the electrode surface up to 1341 s (with the current–time transients beginning to resemble, as shown in Figure 1A). The current of collisions increased as well as the total current because of the accumulation of NPs on the electrode surface.

In the third scenario, when the magnetic field was high (0.2 T), the particles did not reach the electrode surface, which means there was no current related to the occurrence of oxidation processes. These switching modes were applied several times and similar results were obtained. These events can be clearly seen in the presence of a high magnetic field, in which the number of spikes decreased, as shown in Figure 10a. By reducing the applied field to 0.1 T, the particles collided on the surface, increasing the number of spikes as well as the overall the faradaic current (in the interval 1520–1553 s). According to these results, one can infer that it is possible to obtain fine control of the electrochemical process of the NPs-Fe<sub>3</sub>O<sub>4</sub>-PB by modulating the applied magnetic field. Regarding to the results obtained yet, further details should be considered. It is worth mentioned that changing the magnetic field from 0.2 to 0.1 T cause a large jump in the faradaic current, whereas changing it back to 0.2 T does not cause a reversal of this effect (Fig. 9b). We have observed that a fraction still be suspended and reacting on the electrode, however does not produce spikes of current, just faradaic currents.

It is important to discuss the reason background current persists in about 75 nA when the field is again increased to 0.2 tesla. One of hypothesis is based on the scattering experiments; accumulation of nanoparticles result in a larger current and it can also be attributed to the flux of NPs-Fe<sub>3</sub>O<sub>4</sub>-PB. Other possibility is that there are not detection of spikes, it not imply that the particles are not reacting. What support our hypothesis are the decantation experiments monitored *in situ* by light scattering. For the latter, we observe that it is possible that a nanoparticles fraction takes longer to get out of the electrode surface (about 200 minutes). As the electrochemical current transients experiments occurs in a short range of time (e.g. about 100 minutes), this time is not enough for all particles to be removed completely from the suspension. Furthermore, magnetic nanoparticles aggregate in the capillary and out of the capillary after the applying a magnetic field should be considered. In this case we have used the term monodisperse (section 3.1) as a measure of the heterogeneity of sizes of particles. We refer a collection of nanoparticles (based in TEM analysis) monodisperse and uniform, with have the same size, similar shape and mass. However, aggregates can be observed in TEM images; large dispersion in size, shape and

mass distribution (polydisperse or non-uniformity) were not observed. In the case of the experiments reported here, a low concentration of nanoparticles was utilized in order to minimize these effects. Although is expected aggregation in ferromagnetic suspension, this was not a problem to observe the spikes related to the particles collisions.



**Fig. 10** a) Zoomed region between 1510 and 1560 s (with corrected baseline) showing the current–time transients in the presence of a magnetic field. b) Plot of spike current vs. time. The linear regression (red line) shows the decrease in spike intensity with time. 76 spikes were selected from Figure 9a between 0 and 600 s. A baseline current intensity of  $3\sigma$  was used, where  $\sigma$  is the maximum current of the noise.

Other important point to be considered is the possibility that only a tiny proportion of the nanoparticle arrival events that produce, at random, a hugely greater-than-normal current (spike). However, the signal detected for which spike is from the single collision events, in which several particles are detected during the experiments for single events which one. This is interesting for future studies, for example, to identify the influence of charge-transfer for a single particle in different environments. For the latter, physical (or chemical) property of the particle could be modified and then the change on the profile of current-time transient of one spike could be expected.

#### 4. Conclusions

In conclusion, we showed the control of NPs collisions on the electrode surface by applying an external magnetic field. NPs-Fe<sub>3</sub>O<sub>4</sub>-PB with diameters of 10 nm were directed by gravitational force to the electrode surface, and spikes in the current–time transient curves were observed. By using a magnetic field parallel to the electrode surface, the number of nanoparticle collisions and the nanoparticle positions can be controlled, demonstrating that this approach is very promising for fine tuning collision control.

#### Acknowledgments

The authors gratefully acknowledge the financial support from FAPESP (F.N. Crespilho, Project numbers: 2011/01541-0 and 2013/04663-4), CNPq (Project numbers: 304255/2010-6 and 478525/2013-3), INEO, and Nanomedicine Network (NanoBioMed-Brazil, CAPES).

#### Notes and references

† Electronic Supplementary Information (ESI) available: TEM and in situ EDX measurements, and baseline corrected current-time transient for spikes localization. See DOI: 10.1039/b000000x/

#### References

1. X. Xiao and A. J. Bard, *J. Am. Chem. Soc.*, 2007, **129**, 9610-9612.
2. Y. G. Zhou, N. V. Rees and R. G. Compton, *Angew., Chem. Int. Ed.* 2011, **50**, 4219-4221.
3. S. E. Fosdick, M. J. Anderson, E. G. Nettleton and R. M. Crooks, *J. Am. Chem. Soc.* 2013, **135**, 5994-5997.
4. A. Boika, S.N. Thorgaard and A. J. Bard, *J. Phys.Chem. B*, 2013, **117**, 4371-4380.
5. S. E. F. Kleijn, S. C. S. Lai, T. S. Miller, A. I., Yanson, M. T. M. Koper and P. R. Unwin, *J. Am. Chem. Soc.* 2012, **134**, 18558-18561.
6. S. J. Kwon, F. R. F. Fan, and A. J. Bard, *J. Am. Chem. Soc.* 2010, **132**, 13165-13167.
7. X. Y. Xiao, F. R. F. Fan, J. P. Zhou and A. J. Bard, *J. Am. Chem. Soc.* 2008, **130**, 16669-16677.
8. S. J. Kwon, H. Zhou, F. R. F. Fan, V. Vorobyev, B. Zhang and A. J. Bard, *Phys. Chem. Chem. Phys.* 2011, **13**, 5394-5402.
9. X. Y. Xiao, S. L. Pan, J. S. Jang, F. R. F. Fan and A. J. Bard, *J. Phys. Chem. C* 2009, **113**, 14978-14982.
10. H. J. Zhou, F. R. F. Fan and A. J. Bard, *J. Phys. Chem. Lett.* 2010, **1**, 2671-2674.
11. W. Liang, W. Yi, Y. Li, Z. Zhang, M. Yang, C. Hu and A. Chen, *Materials Letters* 2010, **64**, 2616-2619.
12. A. F. A. A. Melo, V. A. N. Carvalho, K. C. Pagnoncelli and F. N. Crespilho, *Electrochem. Commun.* 2013, **30**, 79-82.
13. M. Mason and W. Weaver, *Phys. Rev.* 1924, **23**, 412-426.
14. S. G. Starodoubtsev, E. V. Saenko, A. R. Khokhlov, V. V. Volkov, K. A. Dembo, V. V. Klechkovskaya, E. V. Shtykova and I. S. Zhanavskina, *Microelectron. Eng.* 2003, **69**, 324-329.
15. M. Orellana, P. Arriola, R. Del Río, R. Schrebler, R. Cordova, F. Scholz and H. Kahlert, *J. Phys. Chem. B* 2005, **109**, 15483-15488.